Intensity Attenuation and Enhancement in 3-beam Diffraction *

Ben Post, Po Wen Wang **, and Tommy Hom ***

Z. Naturforsch. **37a**, 528–535 (1982); received March 22, 1982

Dedicated to Herrn Prof. G. Hildebrandt on the occasion of his 60th birthday

A simplified version of the x-ray dispersion surface is described for use in the interpretation of simultaneous 3-beam Borrmann diffraction photographs. Examples of such photographs are discussed and analyzed in terms of the simplified dispersion surfaces.

I. Introduction

Borrmann and Hartwig [1] have shown that the anomalously high transmission of x-rays through perfect crystals in 2-beam diffraction is further enhanced when a third set of planes is brought to its diffracting position. Simultaneous 3-beam diffraction then takes place. That discovery has stimulated large numbers of investigations, in many of which major emphasis has been placed on the spectacular decreases of absorption which often accompany the onset of 3-beam diffraction [2]. Relatively little attention has been paid to the equally significant attenuation of the diffracted intensity which often occurs in 3-beam diffraction and which may result in partial or total eclipse of the anomalous transmission [3]. Observation of these effects requires the use of relatively high resolution techniques [4], which may explain, in part at least, why they have been treated either sketchily or not at all, in the past.

In this paper we discuss these and other factors which influence 3-beam intensities. Four photographs of 3-beam cases in germanium are used to illustrate the 3-beam effects. All three diffracted beams are recorded on each photograph. The enhancements and attenuations of the diffracted intensities will be analyzed qualitatively on the basis of simplified versions of 2 and 3-beam dispersion surfaces.

* Work supported by the National Science Foundation and the Joint Services Electronics Program of the U.S. Defense Department.

** Now with Magnex Corp., San Jose, California, USA.

*** Now with Philips Electronic Instruments, Mahwah, New Jersey, USA.

Reprint requests to Prof. Ben Post, Polytechnic Institute, 333 Jay street, Brooklyn, 11201 New York, USA.

II. Theory

A comprehensive discussion of the theory of n-beam diffraction is given in Ch. 12 of Reference [2]. Useful presentations of the theory, nomenclature and calculation procedures can be found in many of Hildebrandt's papers [5] and in Reference [6]. A brief summary of selected aspects of the theory for centrosymmetric crystals is given below.

In n-beam diffraction, the x-ray wavefields obey Maxwell's equations for a medium with a complex, periodic dielectric constant. A sum of plane waves satisfying Bragg's Law is taken as the assumed solution for the wavefield:

$$\boldsymbol{D} = \sum_{\mathrm{H}} \boldsymbol{D}_{\mathrm{H}} \exp\left[-2\pi i(\boldsymbol{K}_{\mathrm{H}} \cdot \boldsymbol{r})\right]. \tag{1}$$

Using Bragg's Law ($\boldsymbol{K}_{\mathrm{H}} = \boldsymbol{K}_0 + \boldsymbol{H}$), we have

$$\boldsymbol{D} = \exp\left[-2\pi i(\boldsymbol{K}_0 \cdot \boldsymbol{r})\right] \cdot \sum_{\mathrm{H}} \boldsymbol{D}_{\mathrm{H}} \exp\left(-2\pi i \boldsymbol{H} \cdot \boldsymbol{r}\right); \tag{2}$$

$\boldsymbol{K}_{\mathrm{H}}$ is the wave vector within the crystal, directed to reciprocal lattice point H; $\boldsymbol{D}_{\mathrm{H}}$ is the displacement vector, transverse to $\boldsymbol{K}_{\mathrm{H}}$.

A set of linear homogeneous equations for the amplitudes is obtained from the solutions of Maxwell's equations:

$$2\varepsilon_{\mathrm{H}} \boldsymbol{D}_{\mathrm{H}} = -\Gamma \sum_{\mathrm{P}} F_{(\boldsymbol{H}-\boldsymbol{P})} \boldsymbol{D}_{\boldsymbol{P}_{[\mathrm{H}]}}. \tag{3}$$

Equation (3), in a somewhat different form, was first derived by Ewald [7]. $F_{(\boldsymbol{H}-\boldsymbol{P})}$ is a structure factor and $\boldsymbol{D}_{\boldsymbol{P}_{[\mathrm{H}]}}$ the vector component of $\boldsymbol{D}_{\mathrm{p}}$ which is perpendicular to $\boldsymbol{K}_{\mathrm{H}}$. ε is a negative quantity defined by $|\boldsymbol{K}_{\mathrm{H}}| = |\boldsymbol{k}|(1+\varepsilon_{\mathrm{H}})$, k the vacuum wave vector and Γ a constant equal to

$$e^2 \lambda^2 / (4\pi^2 \varepsilon_0 m c^2 V).$$

V is the volume of the unit cell. The other terms have their usual meanings. The summation is over

0340-4811 / 82 / 0600-0528 $ 01.30/0. — Please order a reprint rather than making your own copy.

all reciprocal lattice points, but it is limited in practice to terms for which the ε's are small. The corresponding reciprocal lattice points are then in diffracting position. The permitted values of ε_H are the solutions of the secular determinant of (3). At the exact n-beam point all ε's are equal.

Equation (3) yields n vector equations for n-beam diffraction. It is convenient to decompose each $\boldsymbol{D}_H$ into two mutually perpendicular components, (D_H^σ and D_H^π), in order to deal with polarization effects. It is then necessary to consider 2n scalar equations. The solutions are usually obtained in the form of closely spaced pairs, particularly when the reflections diffract at relatively small Bragg angles. Differences between members of each pair are due to polarization.

The interpretation of the experimental results is simplified if the polarizations of the beams are ignored. The dispersion surface for three beams is then reduced from six to three sheets. The mathematical complications encountered when the solutions of six simultaneous equations are sought tend to obscure the physical processes which take place. These are revealed much more clearly when only three equations need to be dealt with; some loss of precision and detail results, but usually not enough to hamper the analysis.

The determinant of the coefficients of the $\boldsymbol{D}$'s in the expression for 3-beam diffraction is given in (4). It is set equal to zero to avoid trivial solutions.

$$\begin{vmatrix} \left(F_0 + \frac{2\varepsilon_0}{\Gamma}\right) & F_{(-H)} & F_{(-P)} \\ F_{(H)} & \left(F_0 + \frac{2\varepsilon_0}{\Gamma}\right) & F_{(H-P)} \\ F_{(P)} & F_{(P-H)} & \left(F_0 + \frac{2\varepsilon_0}{\Gamma}\right) \end{vmatrix} = 0 . \tag{4}$$

Expansion of the determinant yields a cubic equation:

$$\left(F_0 + \frac{2\varepsilon_0}{\Gamma}\right)^3 - \left(\sum_3 F_i^2\right)\left(F_0 + \frac{2\varepsilon_0}{\Gamma}\right) + 2F_H F_P F_{(P-H)} = 0 . \tag{5}$$

It is convenient to rewrite Eq. (5) in the form:

$$X^3 - AX + B = 0 . \tag{6}$$

For the applications under discussion, the equations yield three real, unequal roots, except for the rare cases where all three structure factors are identical, or where one of the structure factors equals zero. In the former, two roots will have identical values; in the latter, one root will equal zero, and the other two will be equal in magnitude but opposite in sign. In all cases the sum of the three roots must equal zero because of the absence from (6) of a term quadratic in X.

III. Calculations and the Dispersion Surface

The general solutions for the ε's near an n-beam point can be represented by surfaces ("sheets") in reciprocal space. The collection of sheets is the Dispersion Surface. A schematic sketch of a section through a dispersion surface is given in Figure 1. The horizontal lines (1 and 2 to the left, and 2′ and 3 to the right) are the traces, in the plane of the paper, of points which satisfy the general conditions for 2-beam diffraction. At $\Delta\Phi = 0$, the conditions for simultaneous 3-beam diffraction are satisfied. Left-right movement along the horizontal lines corresponds to rotation of the crystal in the opposite sense.

The "Laue" and "Lorentz" lines shown in the figure represent small portions of sections through the corresponding Laue and Lorentz spheres, with radii of $1/(\lambda_{\text{vacuum}})$ and $1/(\lambda_{\text{crystal}})$ respectively: they cross the vertical line at $\Delta\Phi = 0$ at the 3-beam Laue and Lorentz points.

The distance from the Laue to the Lorentz line equals $\frac{1}{2}k\Gamma F_0$ cm^{-1} (defined in Section II). Substitution of F_H for F_0 yields the distance from the corresponding sheet to the Lorentz line. The diffraction angle can be taken into account by multiplying the denominator by cos θ.

To simplify the diagrams, the Laue and Lorentz lines are shown as horizontal lines. The dashed line through the Lorentz point represents the trace, in the plane of the paper, of the surface of the Lorentz sphere at whose center the third reciprocal lattice point is located. The vertical, arrow-tipped lines from the Laue line to the sheet nearest it, determine the "tiepoints" on the latter; these satisfy the surface boundary conditions as well as the general diffraction conditions. The diffracted wave vectors, directed to the relevant reciprocal lattice points, originate at the tiepoints.

The solution of (6) yields three roots, whose magnitudes determine the distances from the Lorentz point to the intersections of the three sheets

with the $\Delta\Phi = 0$ line. The sign of the largest root is positive when the sign of B (in Eq. (6)) is negative; the other two roots then have negative values. The signs of all the roots are reversed when the sign of B (the structure factor triplet phase) is changed.

Substitution of values of sets of germanium structure factors in (6) yields roots which are in good agreement with comparable values derived from calculations which take beam polarizations into account *. To convert the 3-beam roots to reciprocal lattice coordinates, they should be multiplied by $k\Gamma/2\cos\theta_3$, where θ_3 is the 3-beam diffraction angle **.

It is then a simple matter to construct a useful, approximate version of the 3-beam dispersion surface. In Fig. 1, for example, the horizontal 2-beam sheet 1 is made to curve upward to pass through the location of root 1 along $\Delta\Phi = 0$, and then to approach the dashed, sloping Lorentz line asymptotically.

The Borrmann absorption coefficients vary with distance from the Laue line to a given tiepoint. They vanish for tiepoints at the Laue line. They increase monotonically to the average crystal absorption coefficient (μ_0) at the Lorentz line, and continue to increase for tiepoints below the Lorentz line. As a result, most of the observed diffraction intensity originates in tiepoints located in the sheet or sheets nearest the Laue line.

It is useful to discuss the 3-beam roots in terms of four structure factor categories. The corresponding dispersion surface sketches are shown in Figures 1—4.

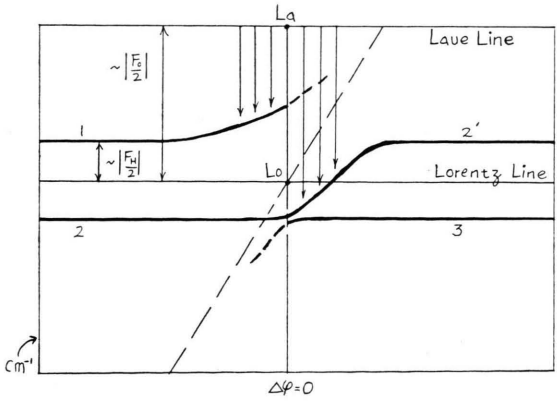

Fig. 1. 3-Beam Dispersion Surface for $F_1 = F_2 = F_3$; Negative Phase.

* See Appendix A. ** See Appendix B.

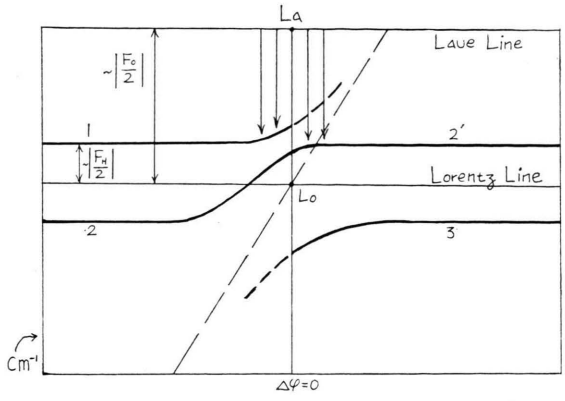

Fig. 2. 3-Beam Dispersion Surface for $F_1 + F_2 = F_3$; Positive Phase.

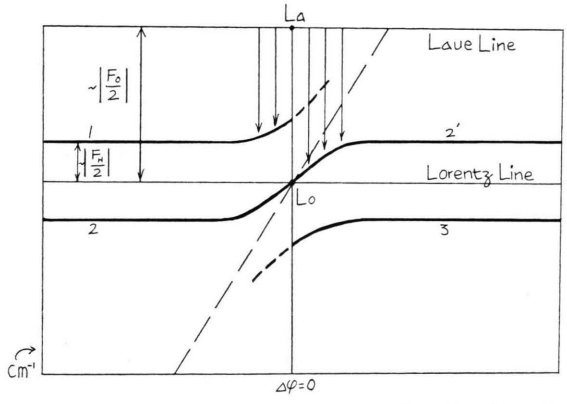

Fig. 3. 3-Beam Dispersion Surface for $F_1 + F_2$; $F_3 = 0$.

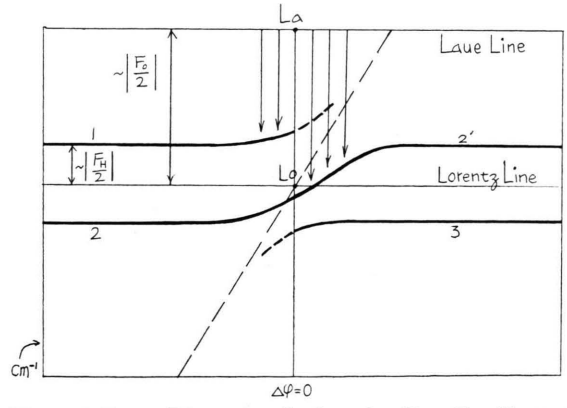

Fig. 4. 3-Beam Dispersion Surface for $F_1 + F_2$; F_3 small. Negative Phase.

1. $F_1 = F_2 = F_3$

For negative B (i.e., negative triplet phase), the 3-beam roots equal $2F$, $-F$, $-F$; the corresponding dispersion surface is shown in Figure 1. To the

left of the 3-beam line ($\Delta\Phi = 0$), the horizontal portion of sheet 1 is characterized by a constant absorption coefficient, which decreases when that line turns upward towards the Laue line. The diffracted intensity increases correspondingly, reaching a maximum at, or very close to the 3-beam line, where the absorption coefficient reaches its minimum value.

To the right of the 3-beam line, as sheet 1 approaches the 1-beam Lorentz line asymptotically, the excitation of the mode decreases rapidly and the absorption coefficient increases and gradually approaches the value μ_0 characteristic of tiepoints along the Lorentz line. In that region (to the right of the 3-beam line), sheet 1 tiepoints no longer satisfy the boundary condition for 2-beam or 3-beam diffraction. The effective tiepoints then lie along the $2-2'$ curve. The absorption increases sharply, accompanied by a decrease or disappearance of the diffracted intensity. Further to the right the absorption gradually decreases to its normal value. The corresponding intensity variation is easily visualized.

For positive B, the largest root is negative. The effects of the change of triplet phase on the dispersion surface are best shown by rotating the entire surface by 180° about the Lorentz line. Sheets 2 and 3 will then be nearest the Laue line. Under those conditions, no substantial intensity variations should be observed accompanying movement across the figure from left to right.

2. $F_1 = F_2 + F_3$

In this case one of the roots will have a magnitude equal to that of F_3. A schematic dispersion surface is shown for this case in Fig. 2, for positive phase. The intensity distribution will differ from case 1 approximately in proportion to the extent to which the magnitude of F_3 differs from those of the other two structure factors (i.e., provided F_1 and F_2 have the same values in both cases).

3. $F_1 + F_2 : F_3 = 0$

Substitution in (6) shows that in this case one root must equal 0. The other two roots have opposite signs, and have magnitudes of $[F_1^2 + F_2^2]^{1/2}$. As shown in Fig. 3, the corresponding dispersion surface will be perfectly symmetrical about the Lorentz point. For the orientation shown, the intensity should increase steadily as the 3-beam setting is approached from the left, due mainly to reduced absorption. It should decrease sharply to the right of the 3-beam line and return gradually to its normal value.

4. $F_1 + F_3 : F_2$ *small*

The intensity distribution should resemble that of case 3. Differences between the two will depend primarily on the extent to which F_3 differs from zero. The corresponding dispersion surface is shown in Figure 4.

IV. Experimental

Divergent microbeam CuK sources were used for all x-ray transmission photographs. Circular targets with diameters of approximately 40 micrometers were used; the effective target size was about 10×40 micrometers at take-off angles of 4 to 8°. The smaller dimension was usually set perpendicular to the plane of incidence to improve resolution in that direction.

Photographs of 3-beam simultaneous diffraction through 0.4 mm thick germanium crystals were obtained. The source to specimen distance was 165 cm. X-ray film cameras were placed about 10 cm beyond the specimen, in position to intercept the three diffracted beams, i.e., the forward diffracted beam (FD), and the two transmitted reflected (TR) beams. Kodak type AA film was used for all exposures. A schematic representation of the experimental arrangement is shown in Figure 5.

The use of a divergent incident beam greatly facilitated the recording of the 3-beam interactions. Alignment of the crystal to within 1 or 2° of the desired setting was usually adequate for our purposes. The corresponding tolerances for highly collimated or monochromatic radiation are usually seconds of arc. The small target made possible the achievement of high resolution without the use of complex and expensive equipment. At 165 centimeters, the source subtends an angle of from 2 to about 8 seconds of arc at points on the specimen surface. An evacuated tube, about 10 cm in diameter, is placed between the source and the specimen to reduce the effects of air absorption. Thin mylar windows at the ends of the tube absorbed less than 20% of the CuKa radiation.

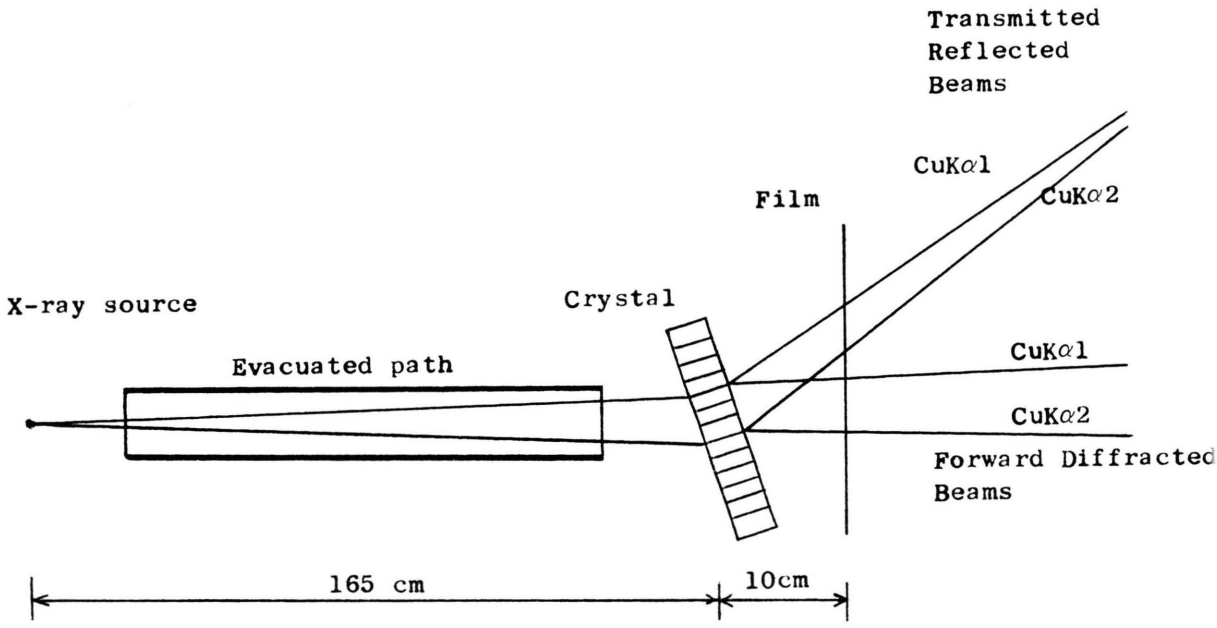

Fig. 5. Schematic Diagram of Experimental Setup.

V. Experimental Results and Discussion

Four photographs showing the intensities diffracted in the course of 3-beam simultaneous diffraction in germanium crystals are discussed in this Section. They illustrate the following cases:

a) (111)/(11$\bar{1}$)/(<u>002</u>)
b) (111)/(002)/(<u>11$\bar{1}$</u>)
c) (111)/(1$\bar{1}\bar{1}$)/(<u>022</u>)
d) (220)/(202)/(<u>02$\bar{2}$</u>)

In each case, the first two reflections refer to the "active" reflections; the third, underlined, is the "coupling" term.

Case a): (111)/(11$\bar{1}$)/(<u>002</u>) (Figure 6)

The dispersion surface corresponding to this case is shown in Figure 3. The structure factor of (002) equals zero. The (111) and (11$\bar{1}$) structure factors are equal and of moderate magnitudes.

Movement along the 2-beam (11$\bar{1}$) line (i.e., along α_1 or α_2) from the left in the F. D. oval, reveals no significant variation of intensity until a point less than 1 minute of arc from the 3-beam point is reached. The intensity then rises sharply to its maximum value at the 3-beam point, and then vanishes just beyond that point. That intensity

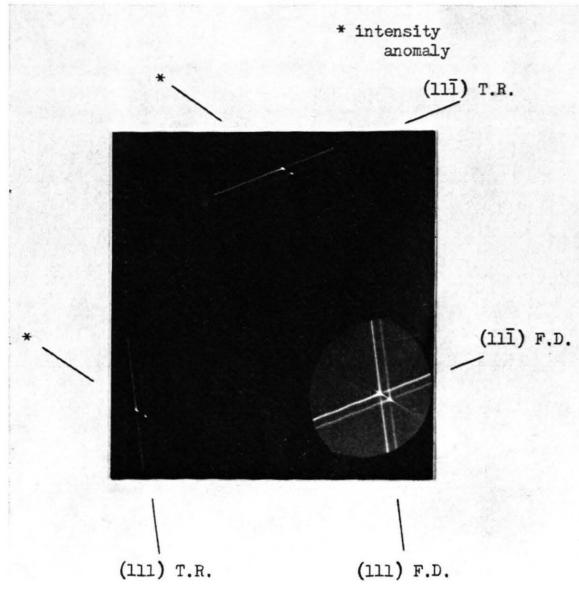

Fig. 6. Photograph: the (111)/(11$\bar{1}$)/(002) case.

eclipse results from the sharp increase in the effective absorption coefficients at settings just beyond the 3-beam setting. This point is discussed in greater detail in [3].

The intensity along $(11\bar{1})$ gradually returns to its normal value within an additional angular interval of about one minute of arc. (The separation of the $CuKa_1$ and Ka_2 lines of the (111) reflections of germanium is very close to two minutes, and provides a useful calibration scale for measurement on the photograph).

The discontinuity in the diffracted intensity is displayed most clearly in the TR portions of the photograph. The streak which extends along the 3-beam line, at the intersections of (111) and $(11\bar{1})$, from Ka_1 to Ka_2 and beyond, is due to the 3-beam enhancement of non-characteristic wavelengths. The intensity of the latter is too low to be visible elsewhere on the photograph. The streak is most noticeable in the FD oval.

Case b): (111)/(002)/($\underline{11\bar{1}}$) (Figure 7)

This case differs from the one immediately preceding as a result of the shift of the (002) from its coupling role in case a to an active role in b. At the exact 3-beam point the two cases are equivalent. They differ along the 2-beam lines. The 2-beam (111) reflection, the 3-beam enhancement, the eclipse, and the faint non-characteristic wavelength streak are all visible in the FD oval. The (002) reflection is, of course, not visible.

In the upper portion of the photograph, the TR record of the (002) line is blank except for the 3-beam enhancement, the latter is displayed in the form of tiny a_1 and a_2 spots. These could constitute a potentially useful source of monochromatic and essentially non divergent radiation.

Case c): (111)/($1\bar{1}\bar{1}$)/(022) (Figure 8)

The corresponding dispersion surface is shown in Figure 2. The photographic record agrees well with predictions based on examination of the dispersion surface.

A minor enhancement of the (111) reflection, which is indicated by the latter, is difficult to detect in the FD region of the photograph due to its similarity to the effects of simple superposition of two reflections. It is, however, readily detected in the TR portions of the photographs. No significant intensity eclipses are expected and none are observed. Differences between the intensities of the TR (111) and the TR ($1\bar{1}\bar{1}$) are due mainly to polarization effects and will not be dealt with here.

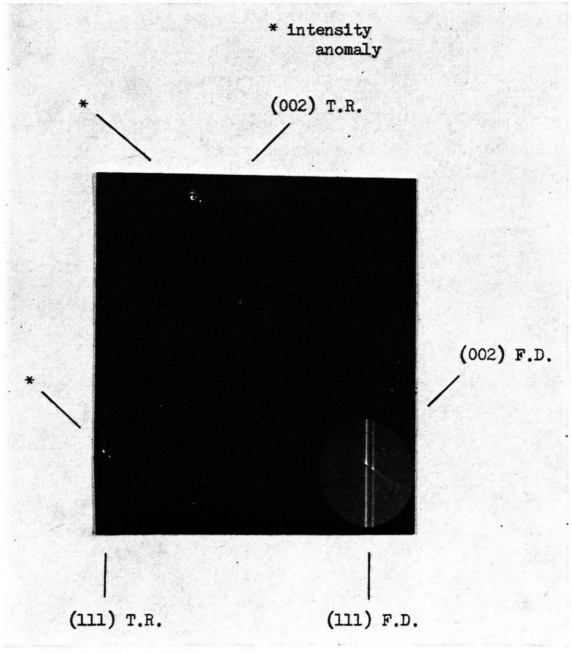

Fig. 7. Photograph: the (111)/(002)/($11\bar{1}$) case.

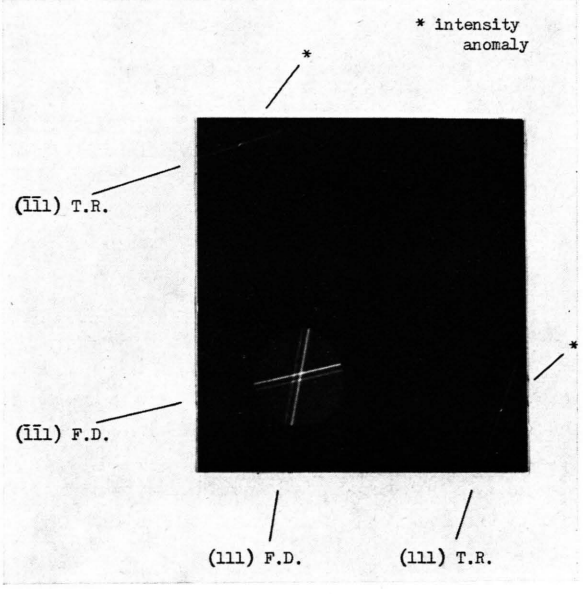

Fig. 8. Photograph: the (111)/($1\bar{1}\bar{1}$)/(022) case.

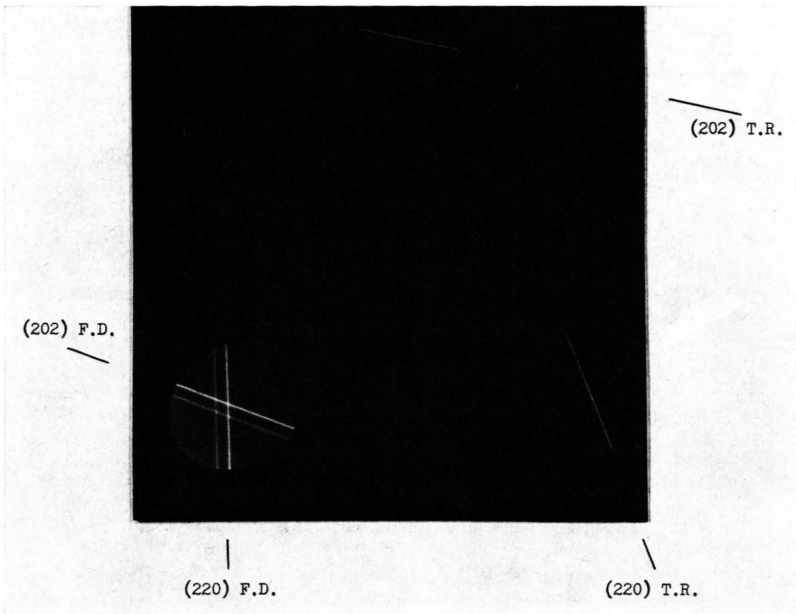

Fig. 9. Photograph: the (220)/(20$\bar{2}$)/(02$\bar{2}$) case.

Case d): (022)/(20$\bar{2}$)/(220) (Figure 9)

The relevant dispersion surface is shown in Figure 1. The latter was calculated for negative phase (i.e., positive largest root). It is therefore necessary to rotate the dispersion surface about the Lorentz line, by 180°, before using it for interpretation of Figure 9. The latter represents a positive triplet phase. It is clear that, for positive phase, lines from the Laue line to tiepoints on sheets 2 and 3 will all be essentially equal in length. No appreciable 3-beam interaction is therefore expected and none is observed.

It should be noted that, in the case of 3-beam diffraction involving strong reflections, such as (220), the magnitude of the largest root may be greater than the separation between the Lorentz and lines, for negative B. It would therefore lie in the region "above" the Laue line. The wavelength to which it would correspond would be less than the vacuum value of the wavelength. That would represent an impossible situation, and the negative phase may therefore be ruled out as a possibility in such cases. This corresponds to one of the well known inequalities of the "Direct Methods" of crystallography, which cause the elimination of negative phases, in similar cases, on purely mathematical grounds.

In summary, we have tried to demonstrate that useful, qualitative interpretations of 3-beam diffraction effects can be based on simplified versions of 3-beam dispersion surfaces, which bypass the mathematical complications of polarization effects.

Appendix A

Values of three roots, for each 3-beam case, are shown in column 1; these are based on solutions of (6). The corresponding six values for each case, based on calculations which take polarization into account, are shown in column 2. The values shown are for germanium crystals and $CuK\alpha_1$ radiation. All values in cm^{-1}.

I. 3-beam case	1	2
I. (111)/(11$\bar{1}$)/(00$\underline{2}$)	158	189
		216
	983	983
		983
		1750
	1808	1777
II. (111)/(1$\bar{1}\bar{1}$)/(0$\underline{2}$2)	300	300
		425
	457	449
		578
		2127
	2336	2307
III. (220)/(022)/(20$\bar{2}$)	306	306
		306
	306	306
		743
		2319
	2540	2319

Appendix B

Consider the transition from 2 to 3-beam diffraction. The 2-beam Bragg angle is determined by the angle between the normal to the diffracting planes and the incident beam direction. The corresponding 3-beam Bragg angle is more critical. It is determined by the angle between the invariant direction of the incident beam and the normal to the plane in which the three relevant reciprocal lattice points lie. We refer to the latter at θ_3.

[1] G. Borrmann and W. Hartwig, Z. Kristallog. **121**, 401 (1965).
[2] Z. G. Pinsker, Dynamical Scattering of X-ray in Crystals, Springer-Verlag, Berlin 1978.
[3] R. Feldman and B. Post, phys. stat. sol., (a) **12**, 273 (1972).
[4] T. C. Huang and B. Post, Acta Cryst. A **29**, 35 (1973).
[5] a) G. Hildebrandt, phys. stat. sol. **24**, 245 (1967). — b) M. Umeni and G. Hildebrandt, phys. stat. sol. (a) **31**, 583 (1975). — c) G. Hildebrandt, Kristall und Technik **13**, 1095 (1978).
[6] B. Post, S. L. Chang, and T. C. Huang, Acta Cryst. A **33**, 90 (1977).
[7] P. P. Ewald, Ann. Phys. **54**, 519 (1917).